Modelling the effect of intervillous flow on solute transfer based on 3D imaging of the human placental microstructure

S. Perazzolo[a,b], R.M. Lewis[b,c], B.G. Sengers[a,b]

[a] *Bioengineering Research Group, Faculty of Engineering and the Environment, University of Southampton, Southampton, SO17 1BJ, UK.*

[b] *Institute for Life Science, University of Southampton, Southampton, SO17 1BJ, UK.*

[c] *University of Southampton, Faculty of Medicine, Southampton, SO16 6YD, UK.*

Corresponding Author: B.G. Sengers (*b.g.sengers@soton.ac.uk)*

Keywords – computational modelling, 3D reconstruction, placenta

Abstract

Introduction: A healthy pregnancy depends on placental transfer from mother to fetus. Placental transfer takes place at the micro scale across the placental villi. Solutes from the maternal blood are taken up by placental villi and enter the fetal capillaries. This study investigated the effect of maternal blood flow on solute uptake at the micro scale.

Methods: A 3D image based modelling approach of the placental microstructures was undertaken. Solute transport in the intervillous space was modelled explicitly and solute uptake with respect to different maternal blood flow rates was estimated. Fetal capillary flow was not modelled and treated as a perfect sink.

Results: For a freely diffusing small solute, the flow of maternal blood through the intervillous space was found to be limiting the transfer. Ignoring the effects of maternal flow resulted in a 2.4 ± 0.4 fold over-prediction of transfer by simple diffusion, in absence of binding. Villous morphology affected the efficiency of solute transfer due to concentration depleted zones. Interestingly, less dense microvilli had lower surface area available for uptake which was compensated by increased flow due to their higher permeability. At super-physiological pressures, maternal flow was not limiting, however the efficiency of uptake decreased.

Conclusions: This study suggests that the interplay between maternal flow and villous structure affects the efficiency of placental transfer but predicted that flow rate will be the major determinant of transfer.

Introduction

The placenta is the interface between the mother and the fetus and adequate placental function is necessary for fetal growth. Placental structure has been shown to be altered in babies who grow poorly in the womb and in response to maternal disease and lifestyle factors [1]. Understanding whether these changes in placental structure help or impair placental function, particularly in terms of gas and nutrient transfer, is an important question. Improved imaging techniques are allowing detailed 3D imaging of the placental villi over wider areas which now allow detailed mathematical modelling of these processes to predict how changes in placental structure may affect placental function.

The human placenta is heamomonochorial, meaning that maternal blood containing the solutes and gases required by the fetus are in direct contact with the fetal tissue [2]. Maternal blood enters the placenta through spiral arteries and percolates through the placental villi for solute exchange to occur. The placental villi form tree like structures, which contain fetal blood vessels surrounded by the placental syncytiotrophoblast, which forms the primary barrier and exchange surface in the placenta. The syncytiotrophoblast forms a selective barrier between the maternal and fetal circulations, transfer of gases occurs by flow limited diffusion, while nutrients and waste products must be transported across the placental barrier. Terminal villi, at the tips of the villous trees, are believed to be the primary site of solute exchange as the diffusion distance between the two circulations is least [3].

Mathematical modelling approaches allow testing of hypotheses in a way which compliments experimental findings, or where experimental approaches are challenging. Previous models of placental transfer have represented very useful 1D, 2D or representative 3D approximations [4-11]. However, the specific 3D morphology of the placenta is likely to play a key role in the overall transfer, both locally at the microscale as well as at the macroscale. Recent advances in imaging technology have allowed 3D image based models to be developed. For example, maternal flow has been modelled to study the shear stress exerted by the maternal blood on the villous surface [12, 13]. However, these studies did not include solute transport. On the other hand, the villous barrier and fetal flow were

modelled to determine the relationship between fetal capillary structure and transfer in the terminal villi [14-16]. However, these studies did not incorporate the maternal flow and instead assumed a fixed solute concentration on the maternal facing surface of the villi, leaving a gap in our knowledge that needs to be investigated further.

The objective of this study is to evaluate the effects of maternal blood flow in the intervillous space on the placental transfer of solutes, modelling both maternal flow as well as solute transport, using 3D image based models of the placental microstructure. With the term solute, we will refer to any small molecular species whose transport mechanism can be described by simple diffusion, e.g. anaesthetics and other gases.

The hydraulic permeability of the maternal circulation associated with the placental microstructure was estimated and the placental uptake was calculated as a measure of transfer for a generic solute. In particular, the effect on uptake was assessed of different maternal blood flow rates below and above the normal physiological range.

Methods

3D reconstruction of the placental microstructure

Tissue was collected from healthy term placentas after delivery with written informed consent and ethical approval from the Southampton and Southwest Hampshire Local Ethics Committee (11/SC/0529).

Samples were collected within 30 min of delivery and villous tissue was dissected and fixed in 4% paraformaldehyde in PBS at 4°C overnight and then stored in PBS at 4°C. Villous fragments were dissected form the fixed tissue and permeabilized in 1% triton X-100 for 2 h, washed in PBS, and incubated overnight with 10 µg/ml Biotin-Datura Starmonium Lectin (DSL, Vector laboratories) which binds specific carbohydrates on the syncytiotrophoblast; 10 µg/ml Rhodamin-Pisum Sativum Agglutinin (PSA, Vector laboratories) which binds specific carbohydrates in the stromal tissue; 10 µg/ml FITC-Aleuria Aurantia Lectinto (AAL, Vector laboratories) which binds specific carbohydrates on the fetal capillary endothelium. Samples were washed in PBS and incubated with Strptavidin-680 (Licor) and 11 nmol/l DAPI for 2 h then washed in PBS. Samples were cleared through a series of 10%, 25%, 50% and 3 x 97%

2, 2'-thiodiethanol (TDE, Fisher Scientific, UK) in PBS for at least 30 minutes per step. Samples were stored in 97% TDE at 4°C until imaging.

The placental villous fragments were imaged with a Leica TCS SP5 laser scanning confocal microscope. For each batch a control sample run without lectin or primary antibody (but including DAPI and any secondary antibodies) was imaged and this sample was used to determine background fluorescence levels for each channel. A series of confocal fluorescence microscopy images were collected from each of six tissue samples with overall dimensions of 0.78 x 0.78 x 0.25 mm (height x width x depth) and a voxel resolution of 0.76 x 0.76 x 1.99 µm (height x width x depth) (Fig. 1A). One additional image sample was collected with dimensions of 1.55 x 1.55 x 0.41 mm (height x width x depth) and a resolution of 1.5 x 1.5 x 4.2 µm (height x width x depth) to test the simulation of even larger sample volumes.

The six 3D image samples were used to evaluate the effects of structural variation. Voxel resolution was reduced to 5 µm in all directions to reduce computational costs in order to enable simulation of the whole image sample volume. To assess the impact of the reduced imaging resolution a sensitivity analysis was carried out in comparison with the original full resolution (Supplementary data). Images were filtered to reduce the background noise (normal Gaussian filter). From the image stack a 3D structure was reconstructed using ScanIP 2016.09-SP1 (Simpleware Ltd, UK). The 3 colour channels in Fig. 1A represent the syncytiotrophoblast (blue), stroma (red) and fetal vessel endothelium (green). Each channel was segmented separately using manual thresholding. Because the syncytiotrophoblast is only a thin layer and due to variations in staining intensity, segmentation did not produce a fully continuous layer. Therefore the syncytiotrophoblast volume was merged with the stroma, representing the overall effective barrier for a small diffusive solute. Similarly, depending on resolution and staining intensity segmentation of the capillary structure displayed local discontinuities and the lumen could not always be distinguished. Therefore, it was assumed that the endothelium was part of the volume of the placental capillaries.

Computational model

The reconstructed 3D solid consisted of three main domains: 1) The intervillous space, i.e., the volume around the villi; 2) The villous barrier, as composed of the syncytiotrophoblast and the stromal layer (DSL+PSA staining); 3) The fetal vessels, represented by the endothelium wrapping the fetal capillaries (AAL staining). Volumetric meshing was carried out by ScanIP 2016.09-SP1 (Simpleware Ltd, UK) after which the model was exported to COMSOL Multiphysics 5.2 (COMSOL Inc., USA). More detail on the model implementation, including a mesh resolution study is provided in the Supplementary data.

Intervillous space blood flow modelling

Fluid flow in the intervillous space was modelled to represent the maternal blood flow percolating around the villi. The fluid was modelled as Newtonian and incompressible. The fluid flow regime was modelled as Stokes flow (creeping flow) in first instance, described by:

$$0 = \nabla[-p\boldsymbol{I} + \mu(\nabla\boldsymbol{u} + (\nabla\boldsymbol{u})^T)] \quad (1)$$

$$\nabla \cdot \mathbf{u} = 0. \quad (2)$$

$\boldsymbol{u}$ and p were respectively the velocity (m/s) and pressure (Pa). μ = 3.2 mPa·s was the dynamic viscosity representative for blood [17]. A pressure difference (P_{in} – P_{out}) of 2.9 Pa was applied along one of the longest dimensions of the sample (L = 0.78 mm) (Figure 1B), based on an estimate of the pressure gradient in the placental cotyledon of 3.7 kPa/m midway along a typical flow path [4, 18]. On the remaining outer surfaces of the sample a no-flux boundary condition was imposed. No-slip boundary conditions were applied for the fluid at the villous boundary walls.

Permeability of the placental structure

The average hydraulic permeability of the placental structures κ (m^2) was estimated according to Darcy's law for porous media:

$$\kappa = a\frac{Q}{\Delta P}, \quad (3)$$

where Q (m^3/s) is the fluid flow and $\Delta P = P_{in} - P_{out}$ (Pa). $\alpha = \mu L/A$, with μ the dynamic viscosity of the fluid (Pa·s), L (m) the length of the sample over which the pressure drop takes place and A (m^2) the cross-sectional area. Q was calculated by integrating the normal fluid velocity over one cross-sectional area. Results were expressed as mean ± SD (N=6). The relationship between permeability and geometrical properties or uptake was represented by Pearson's correlation coefficient r (MATLAB R2016a, 'corr' function).

Solute transfer modelling

The solute transport in the intervillous space was governed by the advection-diffusion equation (Eq. 4), while transport in the villous barrier was governed by diffusion alone.

$$\frac{\partial C}{\partial t} + \nabla \cdot (-D\nabla C) + \boldsymbol{u} \cdot \nabla C = 0. \quad (4)$$

C (mol/m^3) was the solute concentration and D (m^2/s) was the diffusivity of the solute. The diffusivities were considered constant and isotropic. The fluid velocity $\boldsymbol{u}$ was inferred from Eq. 1-2 for the intervillous space, while in the placental barrier $\boldsymbol{u}=\boldsymbol{0}$. For simplicity, we chose just one solute and no solute reactions.

A solute input concentration C_{in} was prescribed as a constant value at the same inlet face as the inflow (Fig. 1B). The initial concentrations in the intervillous space C_{is} and the villous barrier C_{vb} required by COMSOL 5.2 were set to zero (Note however that the problem was solved in steady state). The model did not include blood flow in the fetal vessels, instead the effect of the solute uptake by the fetal capillaries was simplified by constraining the solute concentration in the fetal vessels to zero (perfect sink condition). Thus, fetal vessel concentration C_{fv} was set and maintained constant at zero. No solute metabolism was assumed to occur in each domain. Parameters for oxygen were adopted in Eq. 4 as it is a small solute that moves across the plasma membranes and the connective tissue by simple diffusion [11]. However note that haemoglobin binding kinetics were not included, see discussion. The parameters used in Eq. 4 for the transport of the solute were taken from oxygen literature: C_{in} = 0.1 mol/m^3 [4], and diffusivity in the fluid $D_f = 1.67 \times 10^{-9}$ m^2/s [4].

The model considered the villous barrier as a purely diffusive barrier with $D_{vb} = 0.95 \times 10^{-9}$ m^2/s [19]. Transfer solute across the villous barrier, denoted as uptake q (mol/s), was

calculated as the surface integral of the normal solute flux per area entering the villous barrier surface, based on the internal villous concentration.

The pressure difference was varied over a wide range around the physiological pressure from 1000 fold lower (0.0029 Pa) to 100 fold higher (290 Pa) to study the uptake as a function of the resultant fluid velocity.

An estimate of the total relative placental uptake fraction α_{tot} at the macroscale can be found by taking the average relative uptake (N=6) for the microstructural samples simulated and repeating this over the length of the flow path through the placenta. Relative uptake is defined here as the uptake q divided by the inlet face flux J_{in} (mol/s), i.e. representing the fraction of influx taken up by the placental villi. The cotyledon radius is taken as 1.25 cm [18], therefore 16 samples could be positioned between the cotyledon inflow and outflow. Thus,

$$\alpha_{tot} = 1 - \left(1 - \frac{q}{J_{in}}\right)^{16}. \quad (6)$$

To allow comparison with previous work, an additional test was carried out to evaluate the maximum transfer capacity of the placental barrier alone, neglecting the intervillous space blood flow. The concentration was set constant to C_{in} outside the villous barrier and was kept as a perfect sink condition in the fetal capillaries.

Results

The reconstructed volume of the villi occupied 28 ± 10% of the overall sample volume. The outer surface of the villi was 1.44 ± 0.38 mm^2, while the fetal capillary surface was 0.66 ± 0.29 mm^2, corresponding to a ratio of 2.18 between the outer villous surface and the fetal capillary surface (Table 1). A representative example of simulation results is shown in Fig. 2A. Qualitatively, the flow velocity and the solute concentrations were higher in areas with less dense villi, thus highlighting depleted regions in proximity of denser villous structures (Fig. 2B). The magnitude of the flux through the villous surface showed areas with higher flux capacity (Fig. 2C). Similarly, when the magnitude of the flux entering the fetal capillaries was considered, it showed corresponding areas of higher flux capacity (Fig. 2D). In

combination, these results indicated that villi most protruding in the intervillous space displayed a higher flux capacity compared to the bulk of the villous structure.

Simulation of physiological conditions

The permeability and uptake values under physiological conditions (ΔP = 2.9 Pa) were reported in Table 1. The average hydraulic permeability of the samples was $\kappa = 1.62 \pm 1.35 \times 10^{-9}$ m^2. The average total uptake of the samples was $q = 1.98 \pm 0.83 \times 10^{-12}$ mol/s. Permeability and uptake produced comparable results when simulations were repeated in different directions, i.e. along the other sample dimension of 0.78 mm: $\kappa = 1.33 \pm 1.10 \times 10^{-9}$ m^2, $q = 1.91 \pm 0.67 \times 10^{-12}$ mol/s. Villous volume fractions and villous barrier outer surface showed an inversely proportional trend with permeability (r = -0.68 and r = -0.69 respectively), reflecting the fact that less dense samples have lower resistance to fluid flow. Surprisingly, uptake q was found to be independent from permeability (r = 0.01), despite the lower villous surface area available for uptake in the less dense samples. To investigate this further, also the uptake efficiency of the tissue was evaluated by calculating the uptake per unit of villous volume or surface area. Uptake per unit of villous volume displayed a weak correlation (r = 0.22) with permeability, while uptake per unit of villous outer surface and fetal capillary surface displayed an increasing trend with permeability (r = 0.47 and r = 0.52, respectively).

The average relative uptake of the samples was 22 ± 19 % (N=6), i.e. on average 22% of the solutes entering the sample volume was taken up by the placental structure in steady state. Based on these results, the estimate for macroscale uptake from Eq. 7 gives α_{tot} = 0.98, i.e. on average around 98% of the solute entering the cotyledon would be taken up by the placental villi.

Effect of maternal blood flow rate

Absolute uptake q increased with flow and was observed to level off for high pressure gradients (Fig. 3A). On the contrary, relative uptake showed that the percentage of solute input transferred to the fetus decreased for higher pressure (Fig. 3B).

Simulations reducing the intervillous space pressures generated proportional changes in velocities, as would be expected for Stokes flow, and as a result permeability did not change with pressure. The Reynolds number for the physiological pressures based on a maximum sample dimension of 0.78 mm was 0.26 and the Peclet number was 464. For pressures higher than physiological the full Navier-Stokes equation was used, however differences with Stokes flow remained limited (maximum 4% reduction in permeability, 3% increase in uptake).

Simulation without maternal blood flow

Simulating the villous barrier alone without modelling the maternal flow resulted in an averaged villous uptake of $4.86 \pm 2.57 \times 10^{-12}$ mol/s. Overall, the flux through the villous barrier alone was 2.4 ± 0.4 times higher compared to the simulations with maternal flow under physiological conditions (Fig. 3A).

Simulation of larger structures

An example simulation result under physiological conditions for a 1.55 x 1.55 x 0.41 mm sample was reported in Fig. 4. Qualitatively the same results found for the smaller volume samples appear to be repeated here, i.e. the protruding villi most exposed to the flow displayed higher flux capacities and similar zones of relative solute depletion were found. Permeability and relative uptake were also in the same range as for the smaller samples.

Discussion

This study highlights the importance of the local maternal flow conditions in the placental microstructure for solute transfer to the fetus. By adopting a 3D image based approach this allowed us to model both the detailed flow environment as well as the transport and distribution of solute in the intervillous space. This approach compliments previous studies that have assumed uniform maternal concentrations [14-16]. Testing with uniform maternal concentrations instead of modelling intervillous flow resulted in a 2.4 ± 0.4 times higher uptake and would thus overestimate transfer under physiological flow conditions. This is

further illustrated by the fact that only at very high flow rates simulations with or without flow converged to the same maximum uptake values (Fig. 3A), since intervillous concentrations become uniform.

Flow simulations under physiological conditions resulted in an average blood velocity of 0.1 cm/s in the intervillous space, which is in accordance with previous estimates [10, 12, 18]. Notably, the distribution of solutes in the intervillous space revealed local areas of lower concentrations at steady state (Fig. 2B). This indicated that the villous bulk may hinder flow resulting in more stagnant regions, while the extended villi may be more exposed and favour transfer. Indeed, by studying the uptake capacity of the villous barrier, the extended terminal parts of the villi displayed a larger uptake capacity (Fig. 2C), which would likely be due to a combination of the effects of reduced villous barrier thickness and increased exposure of these villi to the flow. Previous studies have investigated the role of barrier thickness and fetal capillary density [5, 16], but neglected the local effects of maternal flow. Interestingly, placental transfer was found to be relatively constant for samples with widely varying permeability. The reason for this was that less dense microvillous structures had lower surface area available for uptake, but this was compensated by increased flow due to their higher permeability. Indeed, less dense samples displayed increased efficiency with higher uptake per unit of villous area. This indicates that local flow exposure and the occurrence of depleted regions play an important role in the overall efficiency of placental transfer.

Uptake increased with flow, associated with the prescribed pressure gradients and only levelled off at flow rates well above physiological to a constant level determined by the resistance of the villous barrier (Fig. 3A). Thus the maternal flow rate was the main determinant of transfer, in accordance with literature [20]. Note that while for higher flow rates the absolute uptake increased, the overall efficiency of uptake would be reduced, i.e. the relative uptake decreased (Fig. 3B) since the inflow of solutes was so fast that only a smaller fraction could be absorbed by the villi.

Model parameters were based on oxygen due its small size and diffusive nature as well as its biological importance. However, haemoglobin binding kinetics were not considered, so results should be considered representative for a generic small solute. It is

expected that the much larger carrying capacity of haemoglobin would lead to reduced local depletion and a more uniform distribution. Only diffusive transport through the villous barrier was modelled, representing solutes with high membrane permeability. However, by incorporating membrane transporter behaviour (*e.g.* facilitated diffusion), the model could be applied to a wide range of solutes, such as amino acids and fatty acids [9, 21, 22].

Importantly, fetal capillaries were treated as a perfect sink, i.e. kept at zero concentration, which was a first practical assumption that allowed us to estimate the efficiency of the transfer in terms of the maximum possible fluxes across the placental barrier. However, in reality, this represents an over-estimation of the transfer, and could be solved by modelling specifically the fetal placental blood flow [14, 15, 23]. The key factor that determines the effect of this assumption on transfer will be the capillary length until fetal blood saturation is reached. In addition, the assumption of modelling blood as a simple Newtonian fluid should be revisited with a more realistic representation of blood rheology [24].

Samples displayed considerable variability in results, reflecting their differences in structure (Table 1). Modelling larger representative volume sizes (Fig. 4) would reduce the inter sample variability and reduce the effect of the no flux boundary conditions on the local flow pattern and solute distribution, at the expense of greater computational costs. In this respect, the results of varying the imaging resolution and mesh density (Supplementary data) clearly identified the current limitations in terms of accuracy when modelling large samples dependent on the efficiency of the software used and computational resources available, with significant scope for optimisation in the future. In addition, variations in staining intensity pose challenges for the accurate and objective segmentation of confocal imaging data requiring the establishment of robust standardized methodologies and protocols. This includes the effects of tissue fixation on porosity.

While this model represented a generic solute, now that the framework has been established the model can be adapted for any specific solute. We have previously modelled amino acid and fatty acid transport using models which represented membrane transport characteristics but did not include the 3D structure [8, 9]. The geometric and transporter based models could be combined to more accurately represent transport processes and

identify rate limiting processes. Future work could also include the mechanical movement of the villi in the intervillous space, which may adapt and change their positions with the flow rate intensity and direction. The model could be applied to compare normal and altered pregnancies, which may have different transfer efficiencies related both to changes in morphological structures and flow patterns. For example, in preeclampsia or intra uterine growth restriction (IUGR) the pressure in the intervillous space was estimated to be 5 to 10-fold higher [13, 18], and diabetic placentas display distinct differences in structure [25, 26].

In conclusion, modelling placental solute transfer based on 3D imaging of the placental morphology provides a quantitative and diagnostic platform to assess placental transfer of a generic diffusive solute, but which could be adapted for any solute. This will contribute to our understanding of the impact of placental microstructure in health and disease.

Acknowledgements

Imaging in this study was performed with the help of staff and facilities in the Biomedical Imaging Unit, University of Southampton, Faculty of Medicine. SP was funded by an Institute for Life Sciences, University of Southampton PhD studentship and EPSRC DTP. The authors acknowledge the use of the IRIDIS High Performance Computing Facility, and associated support services at the University of Southampton, in the completion of this work. Data for this study will be made openly available from the University of Southampton repository at http://dx.doi.org/10.5258/SOTON/D0270

Conflict of interest

The authors declare that there are no conflicts of interest.

References

[1] R. Lewis, H. Demmelmair, R. Gaillard, K. Godfrey, S. Hauguel-de Mouzon, B. Huppertz, E. Larque, R. Saffery, M. Symonds, G. Desoye, The placental exposome: placental determinants of fetal adiposity and postnatal body composition, Annals of Nutrition and Metabolism 63(3) (2013) 208-215.

[2] A.M. Carter, Evolution of placental function in mammals: the molecular basis of gas and nutrient transfer, hormone secretion, and immune responses, Physiological Reviews 92(4) (2012) 1543-1576.

[3] G.J. Burton, A.L. Fowden, K.L. Thornburg, Placental Origins of Chronic Disease, Physiological Reviews 96(4) (2016) 1509-1565.

[4] I. Chernyavsky, O. Jensen, L. Leach, A mathematical model of intervillous blood flow in the human placentone, Placenta 31(1) (2010) 44-52.

[5] J. Gill, C. Salafia, D. Grebenkov, D. Vvedensky, Modeling oxygen transport in human placental terminal villi, Journal of theoretical biology 291 (2011) 33-41.

[6] M. Lin, B. Mauroy, J.L. James, M.H. Tawhai, A.R. Clark, A multiscale model of placental oxygen exchange: The effect of villous tree structure on exchange efficiency, J Theor Biol 408 (2016) 1-12.

[7] E.M. Lofthouse, S. Perazzolo, S. Brooks, I.P. Crocker, J.D. Glazier, E.D. Johnstone, N. Panitchob, C.P. Sibley, K.L. Widdows, B.G. Sengers, Phenylalanine transfer across the isolated perfused human placenta: an experimental and modelling investigation, American Journal of Physiology-Regulatory, Integrative and Comparative Physiology (2015) ajpregu. 00405.2015.

[8] N. Panitchob, R. Lewis, B. Sengers, Computational modelling of placental amino acid transfer as an integrated system, Biochimica et Biophysica Acta (BBA) - Biomembranes 1858(7-A) (2016) 1451-1461.

[9] S. Perazzolo, B. Hirschmugl, C. Wadsack, G. Desoye, R.M. Lewis, B.G. Sengers, The influence of placental metabolism on fatty acid transfer to the fetus, Journal of Lipid Research (2016) jlr. P072355.

[10] A. Serov, C. Salafia, P. Brownbill, D. Grebenkov, M. Filoche, Optimal villi density for maximal oxygen uptake in the human placenta, Journal of theoretical biology 364 (2015) 383-396.

[11] A.S. Serov, S. C., D.S. Grebenkov, M. Filoche, The role of morphology in mathematical models of placental gas exchange, Journal of Applied Physiology (2015) 543.

[12] E. Lecarpentier, M. Bhatt, G. Bertin, B. Deloison, L. Salomon, P. Deloron, T. Fournier, A.I. Barakat, V. Tsatsaris, Computational Fluid Dynamic Simulations of Maternal Circulation: Wall Shear Stress in the Human Placenta and Its Biological Implications, PloS one 11(1) (2016) e0147262.

[13] C.J. Roth, E. Haeussner, T. Ruebelmann, F.v. Koch, C. Schmitz, H.-G. Frank, W.A. Wall, Dynamic modeling of uteroplacental blood flow in IUGR indicates vortices and elevated pressure in the intervillous space–a pilot study, Scientific Reports 7 (2017).

[14] P. Pearce, P. Brownbill, J. Janacek, M. Jirkovska, L. Kubinova, I. Chernyavsky, O. Jensen, Image-Based Modeling of Blood Flow and Oxygen Transfer in Feto-Placental Capillaries, arXiv (2016).

[15] R. Plitman Mayo, J. Olsthoorn, D. Charnock-Jones, G. Burton, M. Oyen, Computational modeling of the structure-function relationship in human placental terminal villi, Journal of Biomechanics 49(16) (2016) 3780-3787.

[16] R. Plitman Mayo, D.S. Charnock-Jones, G.J. Burton, M.L. Oyen, Three-dimensional modeling of human placental terminal villi, Placenta 43 (2016) 54-60.

[17] P.K. Kundu, I.M. Cohen, Dowling, D.R., Fluid Mechanics, Elsevier Inc., Oxford, UK, 2012.

[18] G. Burton, A. Woods, E. Jauniaux, J. Kingdom, Rheological and physiological consequences of conversion of the maternal spiral arteries for uteroplacental blood flow during human pregnancy, Placenta 30(6) (2009) 473-482.

[19] M.H. Friedman, Principles and models of biological transport, Springer, 2012.

[20] J.J. Faber, Review of flow limited transfer in the placenta, International journal of obstetric anesthesia 4(4) (1995) 230-237.

[21] N. Panitchob, K. Widdows, I. Crocker, M.A. Hanson, E. Johnstone, C. Please, C. Sibley, J. Glazier, R. Lewis, B.G. Sengers, Computational modelling of amino acid exchange and facilitated transport in placental membrane vesicles, Journal of theoretical biology 365 (2015) 352-364.

[22] K.L. Widdows, N. Panitchob, I.P. Crocker, C.P. Please, M.A. Hanson, C.P. Sibley, E.D. Johnstone, B.G. Sengers, R.M. Lewis, J.D. Glazier, Integration of computational modeling with membrane transport studies reveals new insights into amino acid exchange transport mechanisms, The FASEB Journal 29(6) (2015) 2583-2594.

[23] A.T. Shannon, P. Mirbod, Three-dimensional flow patterns in the feto-placental vasculature system of the mouse placenta, Microvascular Research 111 (2017) 88-95.

[24] N. Bappoo, L.J. Kelsey, L. Parker, T. Crough, C.M. Moran, A. Thomson, M.C. Holmes, C.S. Wyrwoll, B.J. Doyle, Viscosity and haemodynamics in a late gestation rat feto-placental arterial network, Biomech Model Mechanobiol 16(4) (2017) 1361-1372.

[25] M. Jirkovská, L. Kubínová, J. Janáček, M. Moravcová, V. Krejčí, P. Karen, Topological properties and spatial organization of villous capillaries in normal and diabetic placentas, Journal of vascular research 39(3) (2002) 268-278.

[26] M. Higgins, P. Felle, E. Mooney, J. Bannigan, F. McAuliffe, Stereology of the placenta in type 1 and type 2 diabetes, Placenta 32(8) (2011) 564-569.

406 *Table 1. Simulation results under physiological conditions.*

Stack number	Villi volume, % of total volume	Villi barrier surface (mm^2)	Capillaries surface (mm^2)	Permeability κ (10^{-10} m^2)	Uptake q (10^{-12} mol/s)	Relative uptake %
1	22	1.35	0.76	20.5	2.77	50
2	25	1.56	0.24	18.6	1.44	4
3	22	0.89	0.42	39.7	1.56	3
4	31	2.06	0.76	6.5	1.97	18
5	49	1.34	0.73	1.5	0.98	38
6	23	1.46	1.06	10.1	3.15	17

407

408

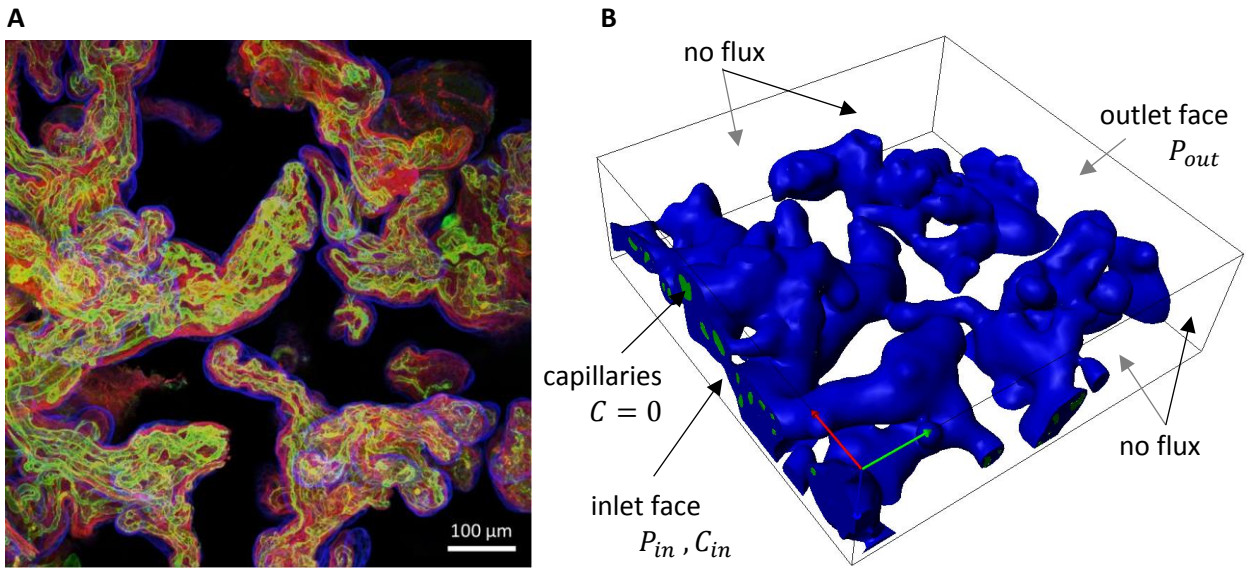

Figure 1. *Examples of confocal imaging and 3D placental reconstruction. (A) Confocal image with tissue specific labelling of the three villous structures. Blue for the syncytiotrophoblast, red for the stroma and green for the fetal vessel endothelium. (B) Segmented image sample showing the 3 domains considered in this study: intervillous space, villous barrier and fetal capillaries (0.78 x 0.78 x 0.25 mm). Pressure and concentration boundary conditions were prescribed for an inflow/inlet face. The outflow/outlet surface is the opposite face of the rectangular sample. P_{in}, P_{out}, are the applied pressure, with $P_{in} > P_{out}$. C_{in}, is the inlet concentration. Capillaries were treated as a perfect sink with $C = 0$. No flux boundary conditions for flow and concentration apply to the remaining surfaces. Here shown is sample 1, the remaining samples can be found in the supplementary data Fig. S1.*

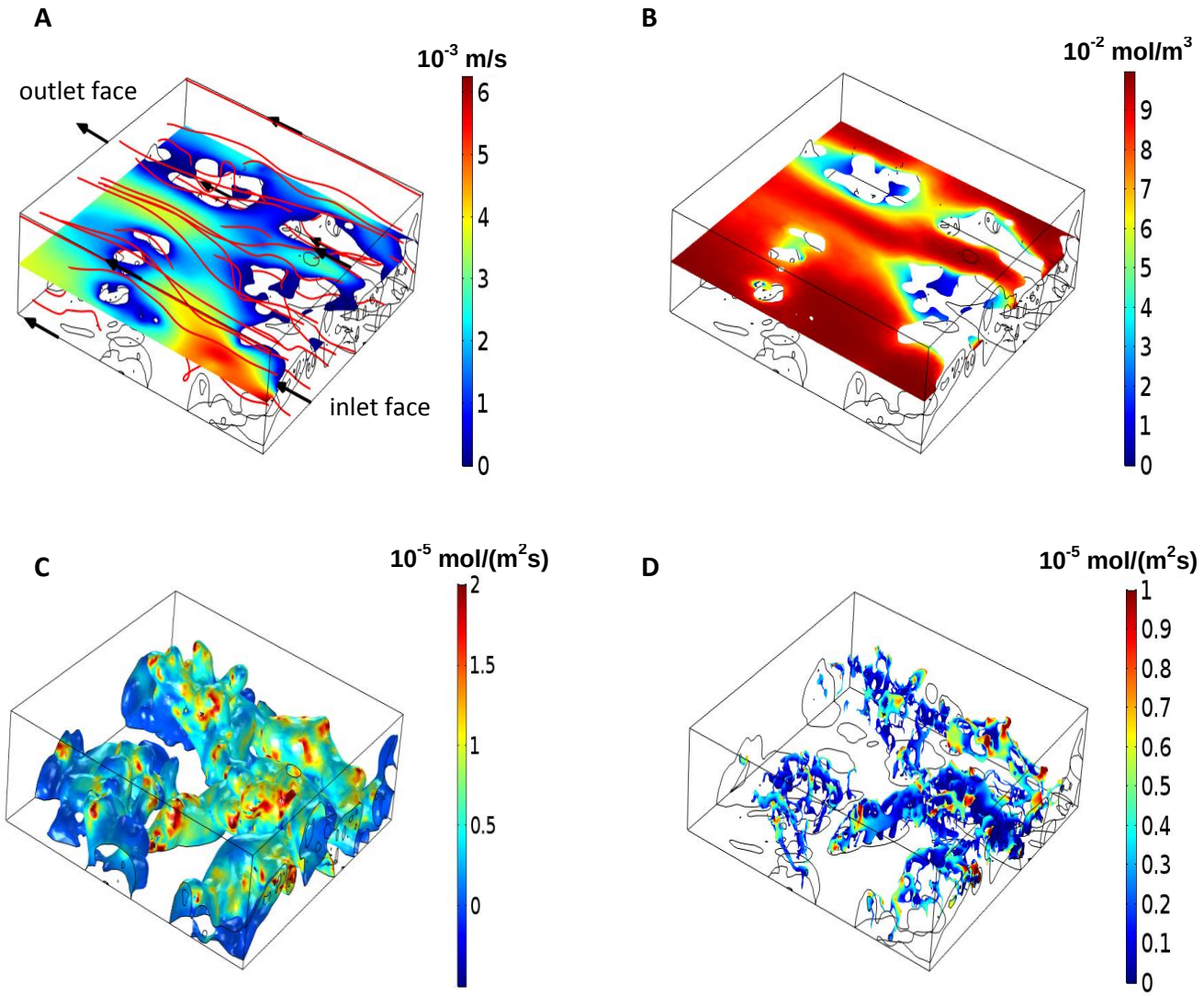

Figure 2. *Example of 3D simulation results modelling flow and solute transport. Shades of red represent higher values, shades of blue represent lower values. (A) Maternal blood absolute velocity field in the intervillous space (m/s) on a plane in the longitudinal direction with streamlines in red depicting the main flow routes (flow direction indicated by black arrows). (B) Corresponding concentration distribution on the same plane in the longitudinal direction (mol/m^3). Blue zones correspond to depleted regions. (C) Solute flux through the villous barrier (mol/(m^{2}s)). (D) Solute flux into the fetal capillaries (mol/(m^{2}s)).*

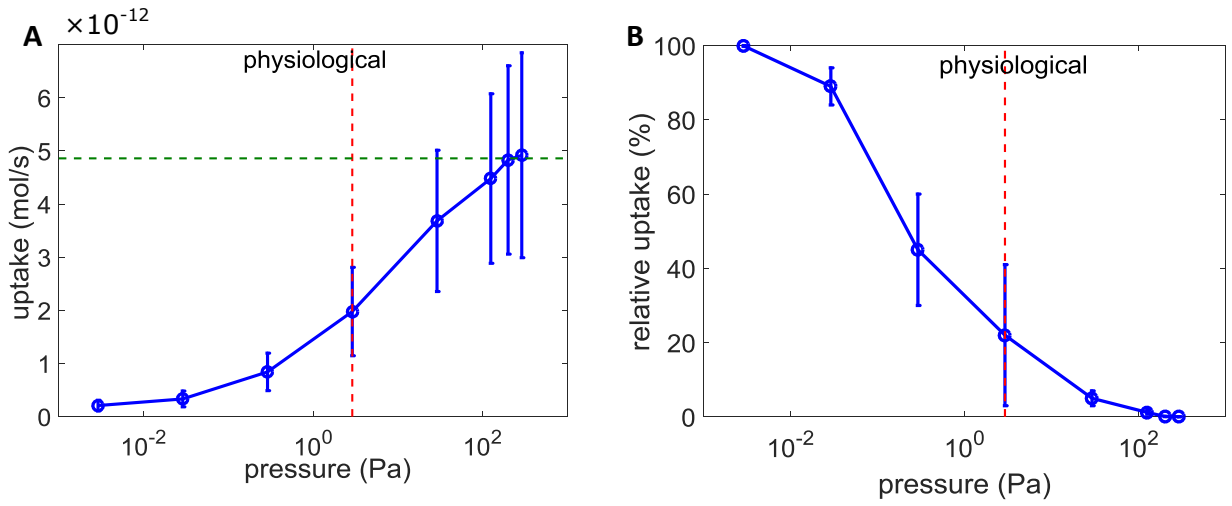

Figure 3. *Uptake as a function of inlet pressure.* (*A) Absolute uptake q (mol/s). The vertical dashed line corresponds to the physiological pressure gradient in the intervillous space. The horizontal dashed line is the average uptake for the simulations of the villous barrier alone without maternal flow. B) Relative uptake as the ratio of the uptake q and the inlet flux, expressed as percentage. All results given as mean ± SD (N=6).*

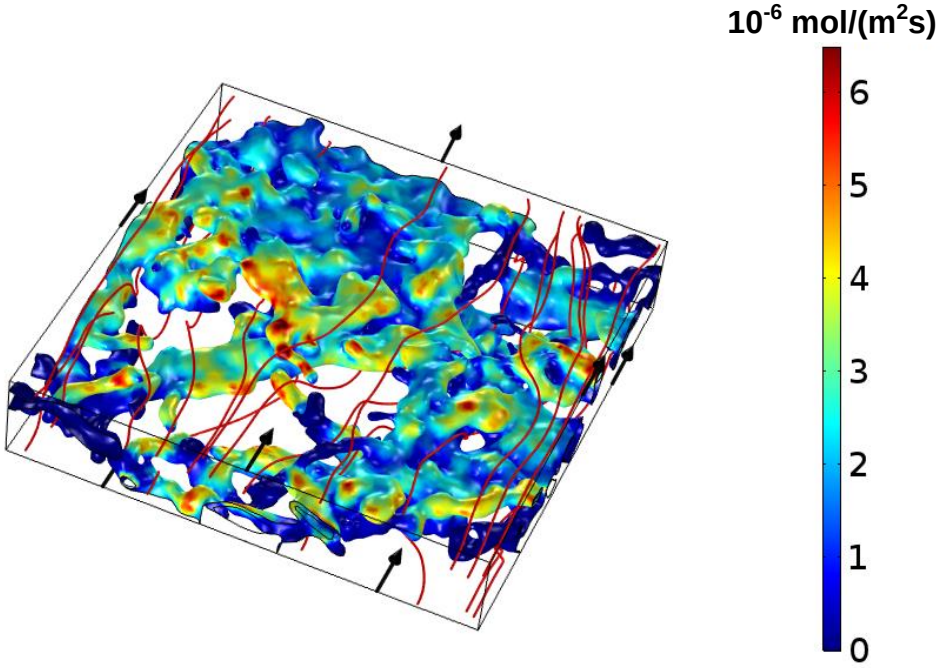

Figure 4. *Example simulation of a larger sample with dimensions of 1.55 x 1.55 x 0.41 mm (*height x width x depth*). Maternal flow streamlines are represented by red lines (direction given by black arrows). Solute flux per unit of area through the villous barrier is mapped with colours corresponding to high (red) and low (blue) flux intensity, respectively.*

Supplementary data:

Modelling the effect of intervillous flow on solute transfer based on 3D imaging of the human placental microstructure

S. Perazzolo, R.M. Lewis, B.G. Sengers

Model implementation

Following segmentation, post-reconstruction smoothing was employed to improve the volumetric meshing. Volumetric meshing was carried out by ScanIP (Simpleware Ltd, UK) with an internal coarseness factor of -50 (coarse mesh) to enable simulation of the whole image sample volume. A sensitivity analysis for the mesh resolution was carried out to evaluate the impact of this setting (see next section below). The mesh was imported into COMSOL Multiphysics 5.2 (COMSOL Inc., USA) where the model was set up for finite element analysis (FEA). Tetrahedral P2+P1 elements were used for the fluid flow problem and linear elements for the convection-diffusion problem. The problem was solved in steady state with the GMRES iterative solver optimized with the Incomplete LU algorithm. Simulations were carried out using the IRIDIS 4 Computing Cluster (University of Southampton, UK) using a 16 core node (2.6 GHz) with 64 GB of memory. For large pressure differences, concentrations in the intervillous space became uniform and it was found this affected the accuracy of the calculated uptake flux when based on external concentrations, therefore uptake was calculated based on the concentration gradient within the villous barrier at all times.

Image and mesh resolution

For the reference simulations in Table 1, the average number of tetrahedral elements was $5.95 \pm 2.66 \times 10^5$ and the run time under physiological conditions was 506±224 min. The impact of image resolution and mesh refinement was evaluated using 6 smaller placental samples (0.2 x 0.2 x 0.2 mm) selected randomly from each of the 6 full (0.78 x 0.78 x 0.25 mm) samples.

The sensitivity analysis demonstrated that reducing the image resolution to 5 µm led to an under-estimate of 7% for the permeability and an under-estimate of 12% for the

uptake compared to full resolution (Table S1), associated with a loss of capillary detail. The mesh coarseness did not have a significant impact on the permeability estimate (Table S2), while using a coarseness setting of -50 led to an over-prediction of the uptake (+18%) compared to the finest mesh evaluated. Note that further mesh refinement is required for uptake to demonstrate convergence, i.e. to see if uptake has fully stabilised.

Table S1. Effect of 3D imaging voxel resolution for six small placental samples (0.2 x 0.2 x 0.2 mm, ScanIP mesh coarseness setting -50). Values reported as mean and standard deviation.

Voxel size (µm)	Number of tetrahedral elements ($\times 10^5$)	Permeability κ ($\times 10^{-9}$ m^2)	Uptake q ($\times 10^{-13}$ mol/s)	Computational time (min)
0.76x0.76x1.99	6.63±2.93	1.23±1.05	5.50±2.41	941±562
2.5	2.63±1.31	1.15±0.92	4.93±2.25	315±201
5	0.91±0.42	1.14±0.93	4.83±2.02	103±56
10	0.46±0.22	1.08±0.87	3.87±1.56	56±37

Table S2. Effect of mesh resolution for the same six small placental samples (0.2 x 0.2 x 0.2 mm, with voxel resolution 5 µm). Values reported as mean and standard deviation.

Mesh resolution (ScanIP mesh setting)	Number of tetrahedral elements ($\times 10^5$)	Permeability κ ($\times 10^{-9}$ m^2)	Uptake q ($\times 10^{-13}$ mol/s)	Computational time (min)
+10 (fine)	9.04±3.12	1.14±0.92	4.10±1.48	1136±474
0	3.92±1.99	1.14±0.92	4.28±1.56	320±179
-25	1.34±0.42	1.14±0.92	4.50±1.72	138±58
-50 (coarse)	0.91±0.42	1.14±0.93	4.83±2.02	103±56

Overview of samples modelled

An overview of the different samples used to evaluate permeability and uptake is given in Fig. S1, in addition to the sample shown in Fig. 1B. The sample numbering corresponds to the results reported in Table 1, e.g. it can be observed that less dense samples have higher permeability.

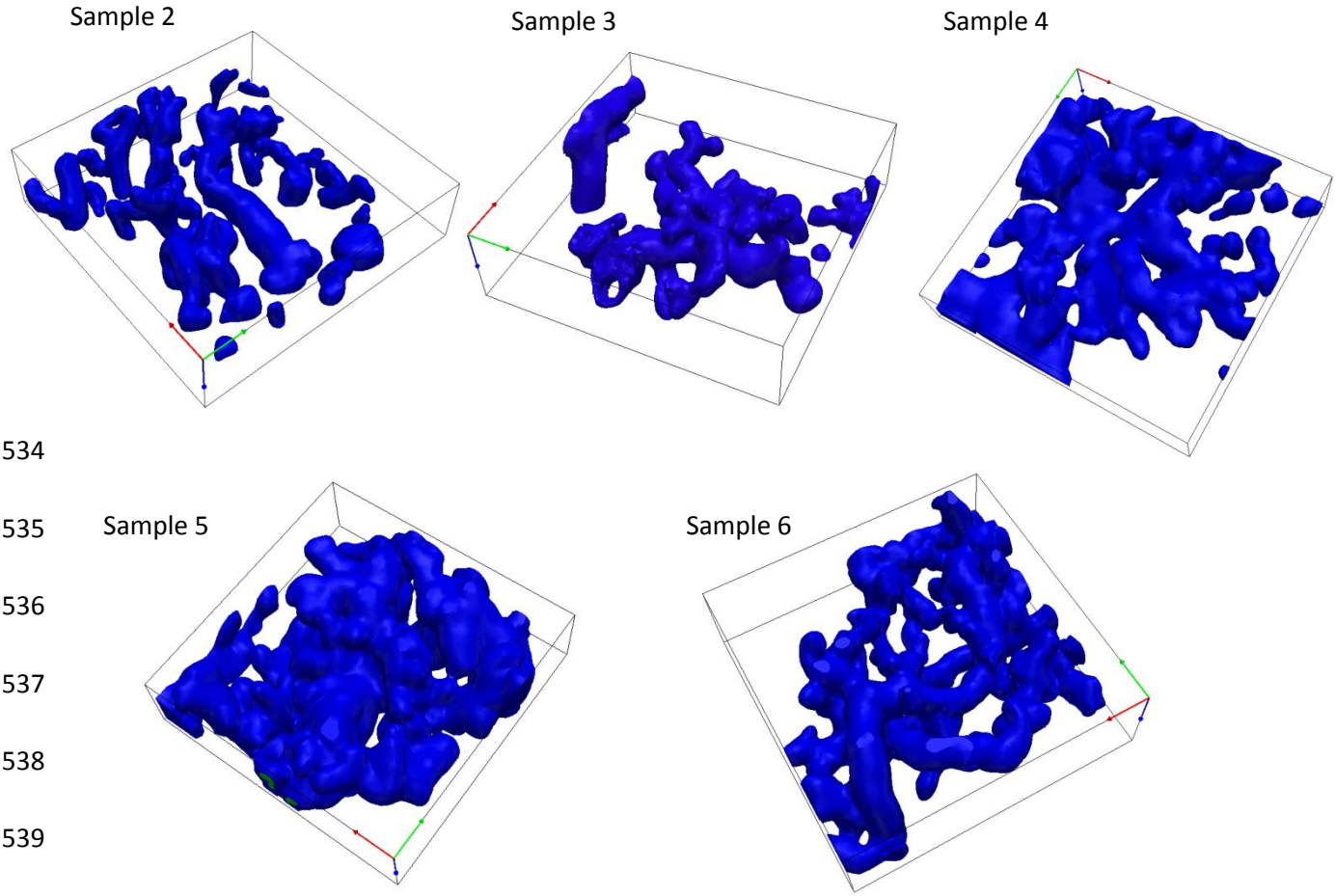

Figure S1. *Overview of samples 2-5 (sample 1 is shown in the main text in Fig. 1B). Segmented images showing the 3D villous microstructure for each sample (0.78 x 0.78 x 0.25 mm).*